750 *Journal of Electrical Engineering & Technology Vol. 6, No. 6, pp. 750~759, 2011*
http://dx.doi.org/10.5370/JEET.2011.6.6.750

Controller Optimization for Bidirectional Power Flow in Medium-Voltage DC Power Systems

Il-Yop Chung†, Wenxin Liu*, David A. Cartes, Soo-Hwan Cho*** and Hyun-Koo Kang§**

Abstract – This paper focuses on the control of bidirectional power flow in the electric shipboard power systems, especially in the Medium-Voltage Direct Current (MVDC) shipboard power system. Bidirectional power control between the main MVDC bus and the local zones can improve the energy efficiency and control flexibility of electric ship systems. However, since the MVDC system contains various nonlinear loads such as pulsed power load and radar in various subsystems, the voltage of the MVDC and the local zones varies significantly. This voltage variation affects the control performance of the bidirectional DC-DC converters as exogenous disturbances. To improve the control performance regardless of uncertainties and disturbances, this paper proposes a novel controller design method of the bidirectional DC–DC converters using L_1 control theory and intelligent optimization algorithm. The performance of the proposed method is verified via large-scale real-time digital simulation of a notional shipboard MVDC power system.

Keywords: Medium voltage DC shipboard power systems, Bidirectional power control, Disturbance rejection, Controller optimization, L_1 theory, Particle swarm optimization

1. Introduction

Direct current (DC) power distribution systems have many advantages over conventional alternating current (AC) systems [1-7]. For example, DC distribution systems can employ fewer power conversions for motor drives and electronic loads than AC systems. DC power converters can also provide significant flexibility in power system control and management. DC distribution systems can provide significant gains in terms of weight, overall cost, manning, and survivability [1-3], especially for electric ship systems. Medium-voltage DC (MVDC) distribution systems are considered promising candidates for next-generation electric shipboard power systems [1, 2].

A notional MVDC shipboard power system has been developed by the Center for Advanced Power Systems at Florida State University (FSU-CAPS) through collaboration with the Electric Ship Research and Development Consortium (ESRDC). The developed system is illustrated in Fig. 1 [8, 9]. The overall MVDC system consists of two main generators, two auxiliary generators, two MVDC buses, and five Zonal Electric Distribution Systems (ZEDS). The propulsion motors and critical loads, such as radars and strategic loads, are connected to the MVDC buses. Energy storage units is deployed in ZEDS to improve energy efficiency and reliability so that surplus energy in the MVDC buses is stored in the energy storages in the ZEDS instead of energy disposal through dynamic braking resistors. The bidirectional DC-DC converters can enable the stored energy to mitigate the peak load or help in black start conditions.

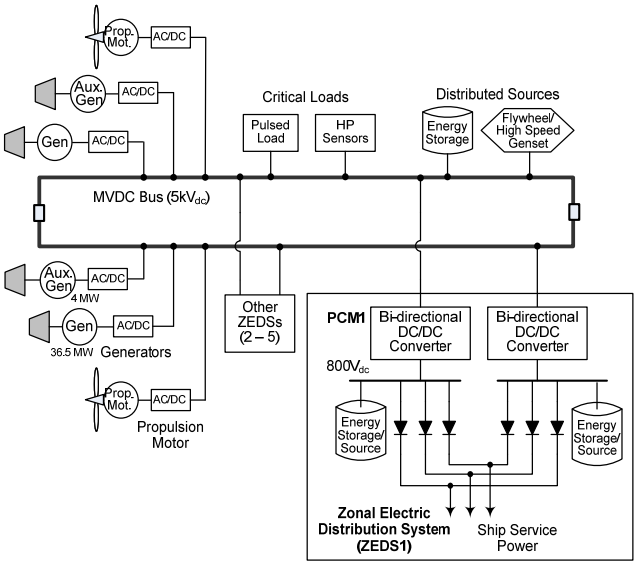

Fig. 1. Single-line diagram of a notional MVDC shipboard power system

† Corresponding Author: School of Electrical Engineering, Kookmin University, Korea. (chung@kookmin.ac.kr)
* School of Electrical and Computer Engineering, New Mexico State University, USA. (wliu@nmsu.edu)
** Dept. of Mechanical Engineering, Florida State University, USA. (dave@eng.fsu.edu)
*** Dept. of Energy Grid, Sangmyung University, Korea (shcho@smu.ac.kr)
§ School of Electrical Engineering, Seoul National University, Korea. (khyun9@powerlab.snu.ac.kr)
Received: October 4, 2010; Accepted: May 30, 2011

In our previous research [8], bidirectional DC–DC converters were developed for the large-scale, real-time MVDC simulation model, whereas the controllers were designed considering time-integrated error minimization. The control performance of the bidirectional DC–DC converter was verified through stability margin analysis and large-scale real-time simulation studies. However, operation of the bidirectional DC–DC converters is easily affected by disturbances and changes in operating conditions. For example, voltage variations of the MVDC or ZEDS can destabilize the bidirectional converters, as well as ZEDS power systems.

This paper focuses on the control method of the bidirectional DC-DC converter that makes the controller more robust to exogenous disturbances and uncertainties. To this end, this paper proposes a novel controller optimization method using L_1 control theory and an intelligent evolutionary technique called particle swarm optimization (PSO). The control performance of the designed bidirectional DC–DC converter is verified with a large-scale Real-time Digital Simulation (RTDS) model of the MVDC system.

2. Bidirectional DC–DC Converter

2.1 Basic operation principle

The configuration of the bidirectional DC-DC converter shown in Fig. 2 was originally proposed by [10]. This configuration has important features for shipboard power systems, such as 1) galvanic isolation with a high frequency (HF) transformer, 2) full-bridge converters on both sides for high-power applications, 3) active clamping circuit for zero-voltage switching, and 4) a current-fed converter on the low voltage side for smoothing power transfer [11-14].

The bidirectional DC–DC converter has two operating modes depending on the power flow direction: buck and boost. In buck mode, electric power is transferred from the high-voltage side to the low-voltage side. The cross-pair switches in the voltage-fed converter [e.g., (S_5, S_6) and (S_7, S_8)] should be switched alternately as shown in Fig. 3(a). When either pair of switches for $D{\cdot}T_S$, are switched on, the line current flows through the switches and the HF transformer. The transferred electric energy charges the inductor in the low voltage side. When the $(1\text{-}D){\cdot}T_S$ gating pulses are switched off, the stored energy in the inductor is discharged and transferred to the ZEDS. The capacitor (C_1) is able to smooth the output voltage. The current-fed converter and the active clamp circuit are turned off in this mode.

In boost mode, electric power flows in the opposite direction. The current-fed converter operates [Fig. 3(b)] while the voltage-fed converter turns off in this mode. During the overlapping period, while all the switches of the

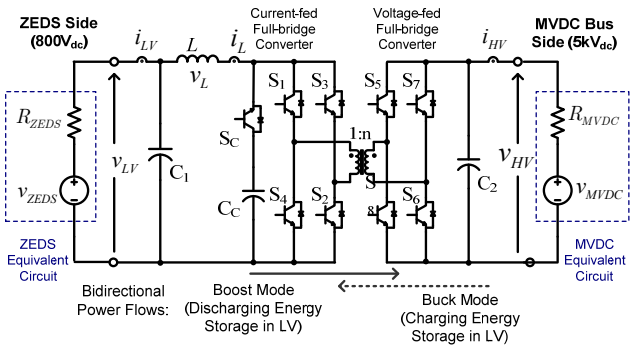

Fig. 2. Electric circuit model of bidirectional DC‑DC converter

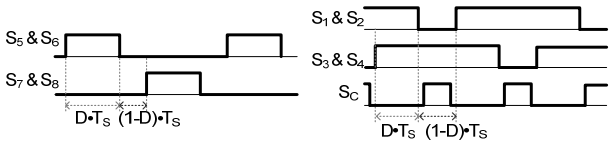

(a) Buck mode gating signal (b) Boost mode gating signal

Fig. 3. PWM gating signal of buck and boost modes

current-fed converter are on, electric energy is charged in the inductor. When any pair of switches turn off, the line current can pass through the HF transformer. The stored energy in the inductor is transferred to the MVDC side. Because voltage transients might occur due to the transformer leakage inductance, the active clamp circuit limits the voltage across the switches and improves the energy efficiency of the converter [10]. A novel active clamping method proposed by [15] has been applied for energy loss reduction in this system.

2.2 Small-signal average model

To analyze system dynamic characteristics, we derived the average model of the bidirectional DC–DC converter. Because the converter switching frequency (f_S) is much higher than the pulse width modulation (PWM) frequency, average models over one switching period (T_S) are sufficient approximation for dynamic analysis and controller design [16]. The obtained average value neglects switching ripples; thus, it varies from one switching period to the next. The average model is obtained by averaging the inductor voltage and the capacitor current on the low-voltage side and applying small-ripple approximation [15]. Reference [8] elaborated the detailed process to obtain the average model of buck and boost modes. From the average model, the small-signal model is obtained as follows.

Buck mode small-signal average model:

$$L\frac{d\hat{i}_L}{dt} = \frac{D}{n}\cdot\hat{v}_{HV} + \frac{V_{HV}}{n}\cdot\hat{d} - \hat{v}_{LV} \tag{1}$$

$$C_1\frac{d\hat{v}_{LV}}{dt} = \hat{i}_L - \frac{\hat{v}_{LV}}{R_{ZEDS}} + \frac{\hat{v}_{ZEDS}}{R_{ZEDS}} \tag{2}$$

Boost mode small-signal average model:

$$L\frac{d\hat{i}_L}{dt} = \hat{v}_{LV} - \frac{D'}{n}\cdot\hat{v}_{HV} + \frac{V_{HV}}{n}\cdot\hat{d} \tag{3}$$

$$C_2\frac{d\hat{v}_{HV}}{dt} = \frac{D'}{n}\cdot\hat{i}_L - \frac{I_L}{n}\cdot\hat{d} - \frac{\hat{v}_{HV}}{R_{MVDC}} + \frac{\hat{v}_{MVDC}}{R_{MVDC}} \tag{4}$$

where d is the duty cycle, R_{ZEDS} and R_{MVDC} are the equivalent resistance of the ZEDS and the MVDC system, i_p is the current of the transformer primary side, n is the transformer turns ratio, D is the steady-state duty cycle, D' is equal to the (1-D), and other variables are noted in Fig. 2. The ^ (hat) notation represents small-signal AC variation around the operating point. The variables in capital letters represent the steady-state values of the operating point obtained as

Buck mode: $V_{LV} = \dfrac{D\cdot V_{HV}}{n}$, $I_L = \dfrac{V_{LV} - V_{ZEDS}}{R_{ZEDS}}$, $I_p = \dfrac{I_L}{n}$ (5)

Boost mode: $V_{HV} = \dfrac{n\cdot V_{LV}}{D'}$, $I_L = \dfrac{n\cdot\left(V_{HV} - V_{MVDC}\right)}{R_{MVDC}\cdot D'}$ (6)

3. Closed-Loop State Space Model

3.1 Feedback control

The control objectives of the bidirectional converter are to regulate the output voltage in buck mode and the output current (or power) in boost mode. Table 1 lists the variables such as control inputs, system outputs, exogenous disturbances, and uncertain parameters of each mode.

Table 1. Variables of the bidirectional DC–DC converter

	Buck mode	**Boost mode**
Input	Duty cycle (d)	Duty cycle (d)
Output	Output voltage (v_{LV})	Output current (i_{HV})
States	Inductor current (i_L) and capacitor voltage (v_{C1})	Inductor current (i_L) and capacitor voltage (v_{C2})
Disturbance	Input voltage (Δv_{HV}) and ZEDS voltage (Δv_{ZEDS})	Input voltage (Δv_{LV}) and MVDC voltage (Δv_{MVDC})
Uncertain parameter	ZEDS equivalent resistance (ΔR_{ZEDS})	MVDC equivalent resistance (ΔR_{MVDC})

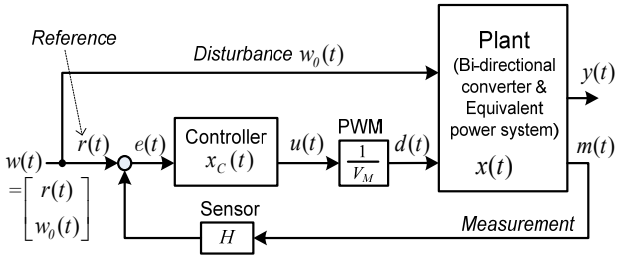

Fig. 4. Closed-loop control block diagram

Fig. 4 shows the simplified closed-loop block diagram of the bidirectional DC–DC converter. The state-space plant models, including the bidirectional DC–DC converter and the MVDC equivalent system, are obtained from (1) to (4). The control input to the plant is generated by the PWM block. The system measurement is fed back to the proportional-integral (PI) controllers with an internal state γ. The controller state equation is written as

$$d = \frac{1}{V_M}\left\{K_p\cdot H\left(r-m\right) + K_i\cdot\gamma\right\} \tag{7}$$

$$\frac{d\gamma}{dt} = -H\cdot m + H\cdot r \tag{8}$$

where the proportional and integral gains are K_p and K_i, respectively; V_M is the magnitude of the PWM carrier wave; and H is the sensor gain.

3.2 Closed-loop state space model

The state model of the plant is written as

$$\dot{x}(t) = Ax(t) + \begin{bmatrix} B_u & B_w \end{bmatrix}\begin{bmatrix} u(t) \\ w(t) \end{bmatrix} \tag{9}$$

$$\begin{bmatrix} m(t) \\ y(t) \end{bmatrix} = \begin{bmatrix} C_m \\ C_y \end{bmatrix}x(t) + \begin{bmatrix} 0 & D_{mw} \\ D_{yu} & D_{yw} \end{bmatrix}\begin{bmatrix} u(t) \\ w(t) \end{bmatrix} \tag{10}$$

where $x(t)$ is the state of the plant; $u(t)$ is the control input; $w(t)$ is the disturbance consisting of the reference input $r(t)$ and the disturbance input $w_0(t)$; $y(t)$ is the performance index; and $m(t)$ is the measured output.

The state model of the controller is obtained as

$$\dot{x}_c(t) = A_c x_c(t) + \begin{bmatrix} B_{cw} & B_{cm} \end{bmatrix}\begin{bmatrix} w(t) \\ m(t) \end{bmatrix} \tag{11}$$

$$u(t) = C_c x_c(t) + \begin{bmatrix} D_{cw} & D_{cm} \end{bmatrix}\begin{bmatrix} w(t) \\ m(t) \end{bmatrix} \tag{12}$$

where $x_c(t)$ is the state of the controller.

From (9) to (12), the closed-loop state-space model of the bidirectional DC-DC converter is written as

$$\dot{\tilde{x}}(t) = A_{cl}\tilde{x}(t) + B_{cl}w(t), \quad \tilde{x}(0) = 0 \tag{13}$$

$$y(t) = C_{cl}\tilde{x}(t) + D_{cl}w(t) \tag{14}$$

where $\tilde{x}(t) = \begin{bmatrix} x(t) & x_c(t) \end{bmatrix}^T$ denotes the closed-loop state vector and the closed-loop matrices are

$$A_{cl} = \begin{bmatrix} A + B_u D_{cm} C_m & B_u C_c \\ B_{cm} C_m & A_c \end{bmatrix}, \qquad B_{cl} = \begin{bmatrix} B_w + B_u D_{cw} \\ B_{cw} \end{bmatrix},$$

$$C_{cl} = \begin{bmatrix} C_y + D_{yu} D_{cm} C_m & D_{yu} C_c \end{bmatrix}, \quad D_{cl} = D_{yu} D_{cw} + D_{yw}.$$

The closed-loop state-space models of the bidirectional DC-DC converter is obtained as follows:

***Buck-mode close-loop state-space model*:** The objective of the buck mode is to control the output voltage v_{LV} to follow the reference input v_{ref}. The performance index, the closed-loop states, and the disturbances are defined as

$$y = \hat{v}_{ref} - \hat{v}_{LV} \tag{15}$$

$$\tilde{x} = \begin{bmatrix} \hat{i}_L & \hat{v}_{LV} & \hat{\gamma} \end{bmatrix}^T \tag{16}$$

$$w = \begin{bmatrix} \hat{v}_{ref} & \hat{v}_{HV} & \hat{v}_{ZEDS} \end{bmatrix}^T \tag{17}$$

where the disturbance w consists of a reference input and two exogenous disturbances such as the input and ZEDS voltage. The closed-loop state-space matrices are obtained from (1)–(2) and (7)–(8) as

$$A_{cl} = \begin{bmatrix} 0 & \left(\frac{-1}{L} - \frac{V_{HV}K_pH}{nLV_M}\right) & \frac{V_{HV}K_i}{nLV_M} \\ \frac{1}{C_1} & \frac{-1}{C_1R_{ZEDS}} & 0 \\ 0 & -H & 0 \end{bmatrix}, \; B_{cl} = \begin{bmatrix} \frac{V_{HV}K_pH}{nLV_M} & \frac{D}{nL} & 0 \\ 0 & 0 & 0 \\ 0 & H & \frac{1}{C_1R_{ZEDS}} \end{bmatrix}$$

$$C_{cl} = \begin{bmatrix} 0 & -1 & 0 \end{bmatrix}, \; D_{cl} = \begin{bmatrix} 1 & 0 & 0 \end{bmatrix} \tag{18}$$

***Boost-mode close-loop state-space model*:** The objective of the boost mode is to control the output current i_{HV} to follow the reference input i_{ref}. The performance index, the closed-loop states, and the disturbances are defined as

$$y = \hat{i}_{ref} - \hat{i}_{HV} = \hat{i}_{ref} - \frac{\hat{v}_{HV} - \hat{v}_{MVDC}}{R_{MVDC}} \tag{19}$$

$$\tilde{x} = \begin{bmatrix} \hat{i}_L & \hat{v}_{HV} & \hat{\gamma} \end{bmatrix}^T \tag{20}$$

$$w = \begin{bmatrix} \hat{i}_{ref} & \hat{v}_{LV} & \hat{v}_{MVDC} \end{bmatrix}^T \tag{21}$$

Similarly, the disturbance w consists of a reference input and two exogenous disturbances such as the input and the MVDC voltage. The closed-loop state-space matrices are obtained from (3)–(4) and (7)–(8) as

$$A_{cl} = \begin{bmatrix} 0 & \left(\frac{-D'}{nL} + \frac{-V_{HV}K_pH}{nLR_{MVDC}V_M}\right) & \frac{V_{HV}K_i}{nLV_M} \\ \frac{D'}{nC_2} & \left(\frac{I_LK_pH}{nC_2R_{MVDC}V_M} - \frac{1}{R_{MVDC}}\right) & \frac{-I_LK_i}{nC_2V_M} \\ 0 & \frac{-H}{R_{MVDC}} & 0 \end{bmatrix}, \; B_{cl} = \begin{bmatrix} \frac{V_{HV}K_pH}{nLV_M} & \frac{1}{L} & \frac{V_{HV}K_pH}{nLR_{MVDC}V_M} \\ \frac{-I_LK_pH}{nC_2V_M} & 0 & \left(\frac{-I_LK_pH}{nC_2R_{MVDC}V_M} + \frac{1}{R_{MVDC}C_2}\right) \\ H & 0 & \frac{H}{R_{MVDC}} \end{bmatrix}$$

$$C_{cl} = \begin{bmatrix} 0 & \frac{-1}{R_{MVDC}} & 0 \end{bmatrix}, \; D_{cl} = \begin{bmatrix} 1 & 0 & \frac{1}{R_{MVDC}} \end{bmatrix} \tag{22}$$

3.3 Eigenvalue analysis

Small-signal models are able to approximate the system dynamics around certain operating conditions. Because of widespread use of power electronic circuits in the MVDC system, small-signal models can provide useful tools to analyze system stability and dynamic performance of the MVDC system [17, 18].

Fig. 5 shows the pole loci of the buck mode according to the changes in the control parameters under the assumption of nominal operation. The figure also shows that the excess increase in the integral gain (K_i) can cause system instability. To avoid this problem, the controller should be tuned carefully.

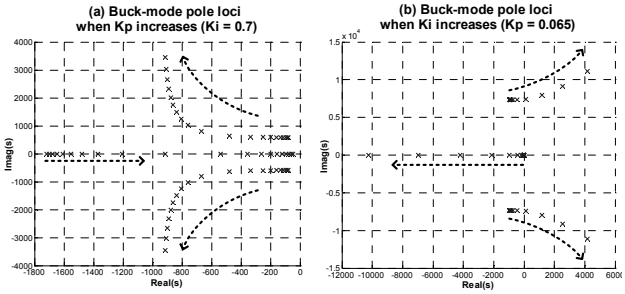

Fig. 5. Root loci of the closed-loop system of the buck-mode according to control parameter changes

Similarly, Fig. 6 shows the pole loci of the boost mode according to (22). The dynamic performance of the boost-mode operation might be poor because the dominant poles are located near the imaginary axis or in the right-half plane. The boost-mode control is difficult because of several factors. One is the non-minimum phase zero of the small-signal transfer function of the bidirectional DC–DC converter, which slackens the control performance because there is undershoot at the beginning of the response [8, 19].

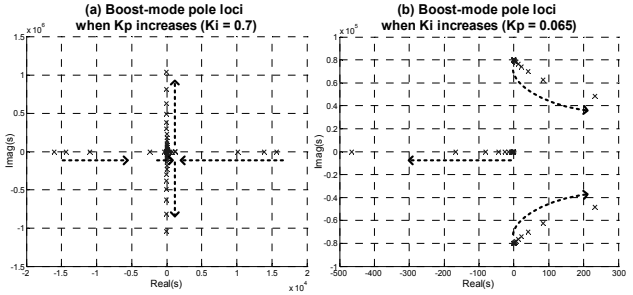

Fig. 6. Root loci of the closed-loop system in the boost-mode (R_{mvdc} = 0.00005 p.u.)

The other issue is related to the line resistance. The boost-mode DC–DC converter is a current-controlled voltage-source converter. This means that the output voltage is manipulated to control the output current. A small line resistance can cause a large increase of the output current in spite of small input variation or disturbances. Fig. 7 shows the modified pole loci of resistance in two lines: 0.00005 and at 0.01 p.u. The pole trajectory of Fig. 7 moves to a more stable area compared to Fig. 6. This means the small resistance in the MVDC

line can improve the stability of the controller. However, increased resistance in the line may increase the energy loss. The line resistance of the MVDC line should therefore be selected carefully.

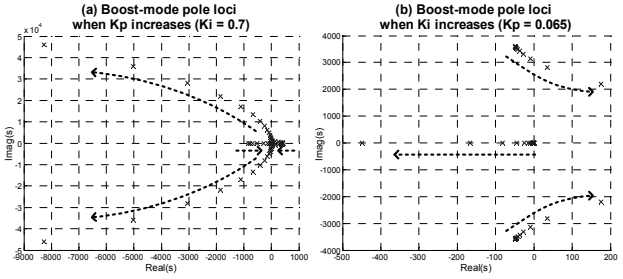

Fig. 7. Root loci of the closed-loop system in the boost mode (R_{mvdc} = 0.01 p.u.)

4. Controller Optimization

4.1 Optimal disturbance rejection

The closed-loop states and outputs are affected by the exogenous disturbance, as shown in (12) and (13). We propose a controller optimization method that can minimize the effect of exogenous disturbances.

To measure the control performance, the performance index y is defined as (15) and (19) in each mode to represent the error between the reference value and the measured value. To achieve optimal disturbance rejection, the performance index y should be minimized against the disturbance w.

Many design theories have been used for optimal disturbance rejection (i.e., H_2 and H_∞ theories] [20-24]. While H_2 theory is based on stochastic white noise disturbance in which the mean is zero, H_∞ theory considers energy-bounded L_2 disturbances. In contrast, L_1 theory considers persistent bounded uncertain disturbances (L_∞ disturbances) [21-24]. Because the disturbances in the MVDC system, such as bus voltage variation, are persistent, L_1 theory is the most relevant in capturing the features of the disturbances.

The L_1 norm of the system's convolution operator G is expressed as (13) and (14) is defined as

$$\|G\|_1 = \max_{w(\cdot)\in L_\infty} \frac{\|y\|_{\infty,\infty}}{\|w\|_{\infty,2}} \tag{23}$$

where $\|y\|_{\infty,\infty} = \max_{-\infty<t<\infty} \|y(t)\|_\infty$ and $\|w\|_{\infty,2} = \max_{-\infty<t<\infty} \|w(t)\|_2$.

The value $\|G\|_1$ can quantify the effect of w (L_∞ disturbance) to y (L_∞ variable). The two definitions of ∞-norms (∞,∞ and $\infty,2$) are used for mathematical convenience to derive the maximum bound of $\|G\|_1$ [23]. From the closed-loop state space model (13–14), the performance variable vector is presented as

$$y(t) = G(t) * w(t) + D_{cl} \cdot w(t) \tag{24}$$

where $G(t) = C_{cl} e^{A_{cl} t} B_{cl}$, $w(t) \in L_{\infty,2}$ and the operator * represents convolution. The norm of the performance variable vector is bounded as

$$\|y\|_{\infty,\infty} \le \|G * w\|_{\infty,\infty} + \|D_{cl} \cdot w\|_{\infty,\infty} \tag{25}$$

According to [23], a positive-definite matrix Q satisfies an algebraic Lyapunov equation:

$$0 = A_{cl} Q + Q A_{cl}^T + \alpha Q + \frac{1}{\alpha} B_{cl} B_{cl}^T \tag{26}$$

where $\alpha > 0$, A_{cl} is Hurwitz and the first term of the right-hand side of (14) are bounded as

$$\|G * w\|_{\infty,\infty} \le \sigma_{max}^{1/2} \left(C_{cl} Q C_{cl}^T\right) \|w\|_{\infty,2} \tag{27}$$

The second term of (25) is also bounded as

$$\begin{aligned} \|D_{cl} \cdot w\|_{\infty,\infty} &= \max_{-\infty<t<\infty} \|D_{cl} \cdot w(t)\|_\infty \le \max_{-\infty<t<\infty} \|D_{cl}\|_{\infty,2} \cdot \|w(t)\|_2 \\ &= \|D_{cl}\|_{\infty,2} \|w\|_{\infty,2} = \sigma_{max}^{1/2} \left(D_{cl} D_{cl}^T\right) \|w\|_{\infty,2} \end{aligned} \tag{28}$$

Therefore, by applying (26) and (28) to (25), we obtain

$$\|G\|_1^2 \le \sigma_{max}\left(C_{cl} Q C_{cl}^T\right) + \sigma_{max}\left(D_{cl} D_{cl}^T\right) \tag{29}$$

Because the algebraic Lyapunov equation of (26) has a positive-definite solution of Q if and only if $A_{cl}+(\alpha/2)I_n$ is Hurwitz, where I_n is an identity matrix, and the positive number α should satisfy

$$0 < \alpha < -2\alpha_R(A_{cl}) \tag{30}$$

where $\alpha_R(A_{cl})$ denotes the spectral abscissa of A_{cl}.

The tightest upper bound for the L_1 norm of the convolution operator G can be obtained as

$$\|G\|_1^2 \le \min_{0<\alpha<-2\alpha_R(A_{cl})} \left\{\sigma_{max}\left(C_{cl} Q C_{cl}^T\right) + \sigma_{max}\left(D_{cl} D_{cl}^T\right)\right\} \tag{31}$$

The control parameters (K_p and K_i) and the positive number α should be chosen to optimize the right-hand side of (31), thereby defining an upper bound on the L_1 norm. Some studies have proposed a gradient-based optimization that requires a differentiable cost function [22, 23]. Because the right-hand side of (22) is not differentiable, Reference [24] applied matrix trace functions. However, the solution process of their methods is complex and results in a more conservative upper bound of $\|G\|_1$.

To optimize the upper bound inherent in (31), we propose a double-layer PSO algorithm. Because the PSO algorithm is based on population-based intelligent optimization, we can obtain the tightest bound without using a trace function. The detailed PSO algorithm will be explained next.

4.2 Controller optimization

The controller design objectives for the bidirectional DC–DC converter are as follows:

- ✓ **Stability criterion**: Undisturbed closed-loop system should be asymptotically stable.
- ✓ **Controller criterion**: Control bandwidth of the bidirectional DC–DC converter should be sufficiently large to follow fast changes in the reference.
- ✓ **Performance criterion**: L_∞ norm of the performance variable *y(t)* should be minimized against persistent, bounded disturbances *w(t)*.
- ✓ **Robustness criterion**: Control performance should be extended to various operating conditions.

The first criterion is achieved by ensuring that the closed-loop system matrix A_{cl} is Hurwitz. The second criterion is related to the pole location of the closed-loop system in *s*-plane. The third criterion is achieved by minimizing (23). For the fourth criterion, the optimization process should cover multiple operating conditions. To find the optimal controller for the objectives, the objective function is defined as

$$J = \sum_{i=1}^{3} c_i \cdot f_i \tag{32}$$

where $f_1 = \begin{cases} 0, & \text{if } A_{cl} \text{ is Hurwitz} \\ 10{,}000, & \text{otherwise} \end{cases}$,

$f_2 = \left| Real(\lambda_C) \right|^{-1}$,

$f_3 = \min_{0<a<-2a_R(A_{cl})} \left\{ \sigma_{max}\left(C_{cl} Q C_{cl}^{\,T} \right) + \sigma_{max}\left(D_{cl} D_{cl}^{\,T} \right) \right\}^{1/2}$,

Here, c_i is the weighting factor and λ_C is the dominant eigenvalue of the closed-loop system; f_1 penalizes for unstable cases and f_2 is to increase controller bandwidth; and f_3 is for optimal disturbance rejection by obtaining the tightest bound of the L_1 norm of *G*.

4.3 Double-layer PSO algorithm

PSO algorithm is applied to optimize the objective function of (32). PSO is a population-based intelligent searching algorithm and has excellent performance for searching the global optimum because it is able to diversify the swarm with a stochastic velocity term [25-26]. The damped reflecting boundary PSO algorithm proposed by [25] is used to improve the PSO boundary problem. The details of the PSO algorithm are found in [26].

Fig. 8 shows the overall optimization process of the proposed double-layer PSO algorithm. Two optimization loops can be used with PSO algorithms. The outer loop (PSO1) finds the control parameters such as [K_p, K_i], whereas the inner loop (PSO2) finds the tightest bound of the L_1 norm depending on [α] for the set of K_p and K_i given by PSO1. The optimization is evaluated in various possible operating conditions to consider robust performance.

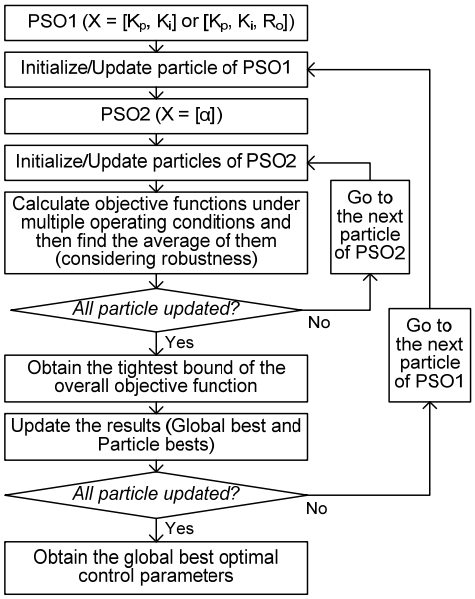

Fig. 8. Double-layer PSO algorithm considering controller design objectives

5. Case Study

The whole MVDC system has been implemented on the RTDS environment, which is specifically designed for electromagnetic transient phenomena of power systems in real time. Fig. 9 shows the 14-rack RTDS systems at FSU-CAPS. Each rack employs multiple processor cards with multiple state-of-the-art microprocessors operating in parallel. The whole MVDC system was simulated in real time with a 93 μs time-step for common components and a 2 μs time-step for switching power electronic components.

Fig. 9. RTDS facility at Florida State University/Center for Advanced Power Systems (FSU-CAPS)

Fig. 10 shows a single-line diagram of the MVDC system emphasizing the ZEDS. The MVDC system utilizes a 5 kV DC ring bus fed from the two 36.5 MW main generators and two 4 MW auxiliary generators. Two propulsion motors are connected to the MVDC bus through DC–AC converters. Five ZEDS of 800 V_{DC} contain various DC or AC ship-service loads. The ZEDS are connected to the MVDC through two power conversion 1 modules (PCM1s), which are bidirectional DC–DC converters. AC loads in the ZEDS, composed of three-phase resistive loads and an induction motor, are fed through the DC-AC converter (PCM2) that can supply 450 V in AC. System parameters and loads of the MVDC system, the bidirectional DC-DC converter, and the ZEDS are listed in Table 2.

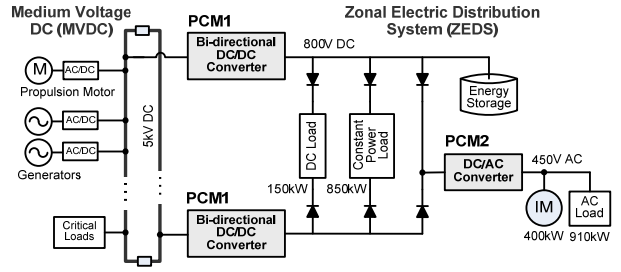

Fig. 10. Single line diagram of ZEDS

Table 2. Parameters of a notional MVDC system for large-scale real-time simulation

Choke inductance (L)	1 mH
Leakage inductance (L_{lk})	27 uH
Transformer turn ratio (n)	3 (1:3)
Switching frequency (f_s)	700 Hz
MVDC voltage (V_{HV})	5 kV
Energy storage voltage (V_{LV})	800 V
Clamp capacitance (C_C)	47 uF
Filtering capacitance (C_1)	2 mF
Filtering capacitance (C_2)	2.7 mF
DC resistive load in ZEDS	150 kW
DC constant power load in ZEDS	850 kW
AC resistive load in ZEDS	910 kW
Induction motor in ZEDS	400 kW
Source and line resistance (R_s)	0.05 Ω
Boost-mode output resistance (R_o)	0.05 Ω

5.1 Case 1: Control performance in buck mode

In this case, the buck-mode operation of the bidirectional DC–DC converter is checked for two operating conditions. The control parameters for buck-mode operation found by the proposed optimization algorithm are K_p=0.0164 and K_i=0.7269. Fig. 11 shows the real-time simulation results using RTDS.

Two operating conditions are tested to prove the performance and disturbance rejection of the optimized controller: one is for PCM1 to supply only the DC load and the other is to supply the induction motor and the AC load through PCM2, as well as the DC load.

The initial condition is to supply only DC loads: the voltage reference of the PCM1 is set to 0.4 kV and the PCM2 is disconnected from the ZEDS. At 1.0 s, the voltage reference changes from 0.4 to 0.8 kV to check the reference tracking control performance. The ZEDS voltage can follow the reference from 0.4 to 0.8 kV without significant transient. Because of the constant power load in the ZEDS, its current decreases while the voltage increases. The reference change causes several transients in the MVDC side; however, there are not very significant.

The operating condition changes. The induction motor and the AC load are activated, and PCM2 starts supplying power at 11.0 s, as shown in Fig. 11. This test is to check the effect of load change. Several transients are apparent in the ZEDS and MVDC voltage; however, these they are eliminated by the control action.

As shown in Fig. 5, the buck-mode control is relatively stable. The simulation results with the control parameter tuned by the heuristic approach also showed good performance; thus, these data were omitted from the current study.

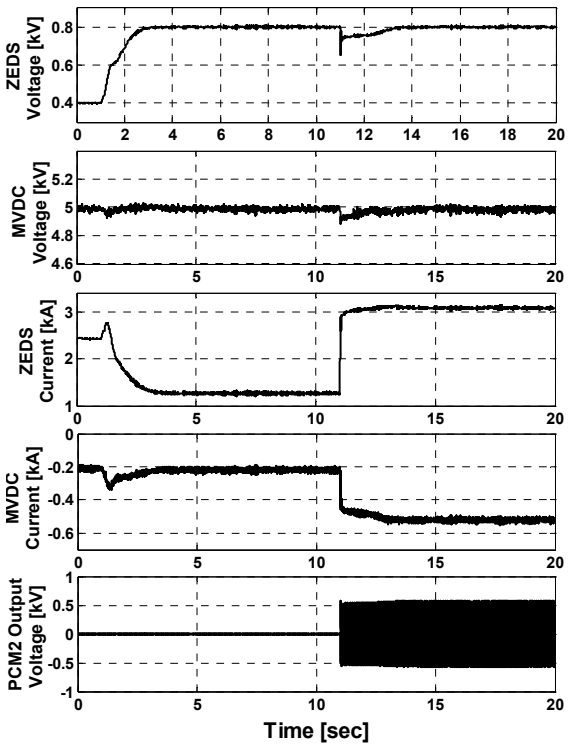

Fig. 11. RTDS simulation result of buck-mode operation of bidirectional DC–DC converters when obtained optimal control parameters (K_p=0.0164 and K_i=0.7269) are applied

5.2 Case 2: Control performance in boost mode

The boost-mode operation of the bidirectional DC-DC converter is tested for two controllers. One controller is tuned by a conventional method that uses a heuristic

method considering transient performance and error minimization (K_p=0.0056, K_i=5.0). Fig. 12 shows the real-time simulation result of the conventional method. The other is optimized by the proposed method based on four criterions defined in Section 4.2 (K_p=0.15, K_i=4.1). Two operating conditions (i.e., normal and line fault) are also tested to check the robustness and control performance.

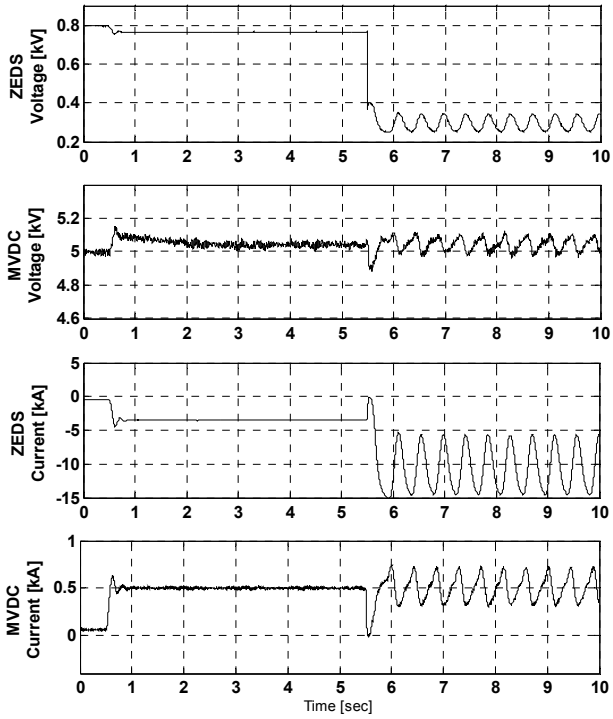

Fig. 12. RTDS simulation result of boost-mode operation of bidirectional DC-DC converters for conventionally-tuned control parameters (K_p=0.0056 and K_i=5.0)

The initial simulation condition is that the output current reference of the boost-mode bidirectional converter is set to 0.0 kA and the energy storage discharges power to supply the ZEDS. At 0.5 s, the reference current changes from 0.0 to 0.5 kA. Both controllers are able to track the reference current fairly well, even though there are some overshoot in the heuristically tuned controller in Fig. 12 compared to Fig. 13. The output current in the MVDC side is controllable at 0.5 kA, which also means the bidirectional DC–DC converter controls the output power at 2.5 MW.

At 5.5 s, a fault occurs in the ZEDS side such that the ZEDS voltage instantly drops more than 0.4 kV. This checks the disturbance rejection performance of the controllers. In Fig. 12, significant oscillations occur nearly everywhere (i.e., all the current and voltage waveforms at both MVDC and ZEDS sides). The oscillation in the MVDC bus voltage is able to propagate instantly all over the shipboard power system because most power equipments are connected to the MVDC bus. This voltage oscillation can cause severe power quality problems, stresses in power devices and so on.

Fig. 13 shows that the controller optimized by the proposed method can control the output current well around the reference value of 0.5 kA even after the fault. Although there is a transient immediately after the fault, the controller is able to reject the disturbances and maintain good control performance. No significant oscillation occurs in the current and voltage waveforms, even though there is some transient immediately after the fault. The MVDC voltage can also be maintained more efficiently because the faults in local ZEDS are isolated and the rest of the system are protected from the impact of the faults. The proposed method minimizes the effect of the exogenous disturbances, such as voltage variations, in both sides and the operating condition changes are reflected on the reference current, as defined in (21). Therefore, the proposed method is capable of excellent performance for disturbance rejection against the operating conditions changes and disturbances.

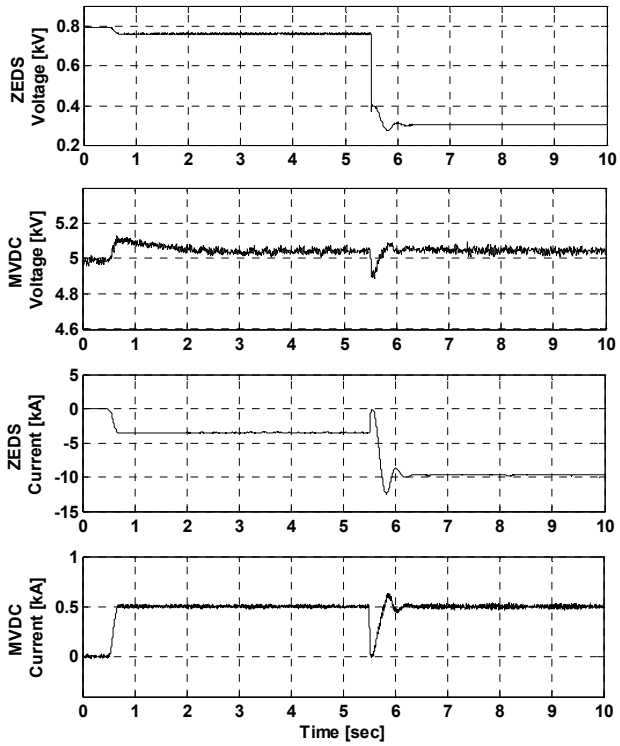

Fig. 13. RTDS simulation result of boost-mode operation of bidirectional DC-DC converters for the proposed control parameters (K_p=0.15 and K_i=4.1)

6. Conclusions

Because shipboard power systems have limited resources in limited space, the control objectives are more rigorous than terrestrial power systems. Bidirectional DC–DC converters in the MVDC system suffer severe disturbances that may cause significant degradation in control performance. In the current study, an advanced control method using L_1 theory and PSO algorithm to

reject the voltage disturbances at the input and output stages was discussed. The disturbance rejection performance was quantified by using the L_1 norm of the convolution operator between the performance index and the disturbances. In the proposed method, multiple criteria in terms of stability, control bandwidth, disturbance rejection, and robustness are considered simultaneously in the optimization process. The proposed control performance has been verified through large-scale real-time system simulation using RTDS.

Acknowledgments

This work was supported by the 2011 Research Program of Kookmin University in Korea and the MKE (The Ministry of Knowledge Economy), Korea, under the ITRC (Information Technology Research Center) support program supervised by the NIPA (National IT Industry Promotion Agency) (NIPA-2011-C1090-1121-0005) and the Basic Science Research Program through the National Research Foundation of Korea (NRF) funded by the Ministry of Education, Science and Technology (2011-0014872).

References

[1] J.G. Ciezki and R.W. Ashton, "Selection and Stability Issues Associated with a Navy Shipboard DC Zonal Electric Distribution System," IEEE Trans. on Power Delivery, vol. 15, no. 2, Apr. 2000, pp.665-669.

[2] N. Doerry, "Next Generation Integrated Power Systems (NGIPS) for the Future Fleet," IEEE Electric Ship Technologies Symposium 2009.

[3] E. Zivi, "Design of robust shipboard power automation systems," Annual Reviews in Control, vol. 29, issue 2, 2005, pp.261-272.

[4] A. Sannino, G. Postiglione, and M.H. Bollen, "Feasibility of a DC Network for Commercial Facilities," IEEE Trans. on Industry Applications, vol. 39, no. 5, Sep-Oct. 2003, pp. 1499-1507.

[5] M.E. Baran and N.R. Mahajan, "DC distribution for industrial systems: opportunities and challenges," IEEE Trans. on Industry Applications, vol. 39, issue 6, Nov-Dec. 2003, pp. 1596 – 1601.

[6] D. Salomonsson and A. Sannino, "Low-Voltage DC Distribution System for Commercial Power Systems With Sensitive Electronic Loads," IEEE Trans. on Power Delivery, vol. 22, no. 3, Jul. 2007, pp. 1620-1627.

[7] E. de Jong and P. Vaessen, "DC power distribution for server farms," KEMA Consulting (http://www.leonardo-energy.org), Sep. 2007.

[8] I. Chung, W. Liu, S. Leng, M. Andrus, D.A. Cartes, M. Steurer and K. Schoder, "Integration of a bidirectional DC–DC converter model into a large-scale system simulation of a shipboard MVDC power system," in Proc. IEEE ESTS, Apr. 20–22, 2009, pp. 318–325.

[9] M. Adrus, M. Steurer, C. Edrington, F. Bogdan, H. Ginn, R. Dougal, E. Santi, and A. Monti, "Real-time Simulation-based Design of a Power-Hardware-In-The-Loop Setup to Support Studies of Shipboard MVDC Issues," in Proc. IEEE ESTS, Apr. 20–22, 2009, pp. 142-151.

[10] K. Wang, F. C. Lee, and J. Lai, "Operation Principles of Bidirectional Full-bridge DC/DC Converter with Unified Soft-Switching Scheme and Soft-Starting Capability," IEEE-APEC Conf. pp. 111-118, 2000.

[11] J. Lai and D.J. Nelson, "Energy Management Power Converters in Hybrid Electric and Fuel Cell Vehicles," Proceeding of the IEEE, vol. 95, no. 4, pp. 766-777, Apr. 2007.

[12] S. Inoue and H. Akagi, "A Bidirectional DC–DC Converter for an Energy Storage System With Galvanic Isolation," IEEE Trans. on Power Electronics, vol.22, no.6, pp. 2299-2306, Nov. 2007.

[13] R.W. De Doncker, D. M. Divan, and M. H. Kheraluwala, "A three phase soft-switched high-power density DC/DC converter for high-power applications," IEEE Trans. Ind. Appl., vol. 27, no. 1, pp. 63–73, Jan./Feb. 1991.

[14] H. Chiu and L. Lin, "A Bidirectional DC–DC Converter for Fuel Cell Electric Vehicle Driviing System," IEEE Trans. on Power Electronics, vol.21, no.4, pp.950-958, Jul. 2006.

[15] E. Park, S. Choi, J. Lee, and B.H. Cho, "A soft-switching active-clamp scheme for isolated full-bridge boost converter," IEEE-APEC Conf. 2004, vol. 2, pp. 1067-1070, 2004.

[16] R.W. Erickson and D. Maksimovic, Fundamentals of Power Electronics, Second Ed. Springer, 2001.

[17] J. Sun, "Small-Signal Methods for Electric Ship Power Systems," in Proc. IEEE ESTS, Apr. 20–22, 2009, pp. 44-52.

[18] S.R. Rudraraju, A.K. Srivastava, S.C. Srivastava, and N.N. Schulz, "Small Signal Stability Analysis of A Shipboard MVDC Power System," in Proc. IEEE ESTS, Apr. 20–22, 2009, pp.135-141.

[19] S. Arulselvi, G. Uma, and M. Chidambaram, "Design of PID Controller For Boost Converter with RHS Zero," The 4th International Power Electronics and Motion Control Conference (IPEMC), vol.2, pp. 532-537, 2004.

[20] J.B. Burl, Linear Optimal Control – H2 and H∞ Methods, Addison-Wesley, 1999.

[21] M. Vidyasagar, "Optimal Rejection of Persistent Bounded Disturbances," IEEE Trans. Automatic Control, vol. AC-31, no. 6, pp. 527-534, Jun. 1986.

[22] W.M. Haddad, and V. Chellaboina, "Mixed-Norm H2/L1 Controller Synthesis via Fixed-Order

Dynamic Compensation: A Riccati Equation Approach," Proceedings of the 36th Conference on Decision & Control, pp. 452-457, Dec. 1997.
[23] V.S. Chellaboina, W.M. Haddad, and J.H. Oh, "Fixed-order dynamic compensation for linear systems with actuator amplitude and rate saturation constraints," International Journal of Control, vol. 71, no. 12, pp/1087-1103, 2000.
[24] T.D. Curry, and E.G. Collins, Jr., "Robust l1 design of a multivariable PI controller using a real-coded genetic algorithm," Proceedings of the 2005 American Control Conference, vol. 6, pp. 4295-4300, 8-10 Jun. 2005.
[25] J. Robinson and Y. Rahmat-Samii, "Particle swarm optimization in electromagnetics," IEEE Trans. Antennas and Propagation, vol.52, no.2, pp.397-407, Feb. 2004.
[26] I. Chung, W. Liu, D.A. Cartes, and K. Schoder, "Control Parameter Optimization for a Microgrid System Using Particle Swarm Optimization," IEEE International Conference on Sustainable Energy Technologies (ICSET 2008), Singapore, Nov. 2008.

Il-Yop Chung received his BS, MS, and PhD degrees in Electrical Engineering from Seoul National University, Seoul, Korea, in 1999, 2001, and 2005, respectively. He was a Postdoctoral Associate at Virginia Polytechnic Institute and State University, Blacksburg, VA, USA from 2005 to 2007. He was also a Visiting Researcher at ABB US Corporate Research Center, Raleigh, NC, USA in 2007. From 2007 to 2010, he worked for the Center for Advanced Power Systems (CAPS) at Florida State University, Tallahassee, FL, USA as a Postdoctoral Associate and Assistant Scholar Scientist. Currently, he is a professor at Kookmin University, Seoul, Korea. His research interests are power quality, distributed energy resources, renewable energy, and shipboard power systems.

Wenxin Liu received his PhD degree in Electrical Engineering from Missouri University of Science and Technology (formerly University of Missouri-Rolla), Rolla, MO, USA in 2005. He received his BS and MS degrees from Northeastern University, China in 1996 and 2000, respectively. From 2005 to 2009, he was an Assistant Scholar Scientist with the Center for Advanced Power Systems (CAPS) at Florida State University, Tallahassee, FL, USA. He is currently an Assistant Professor with the Klipsch School of Electrical and Computer Engineering at New Mexico State University, Las Cruces, NM, USA. His current research interests include neural network control, swarm intelligence, control and optimization of microgrids, and renewable energy.

David A. Cartes received his PhD degree in Engineering Science from Dartmouth College, Hanover, NH, USA. Since January 2001, he has been an Associate Professor in the Department of the Mechanical Engineering, Florida State University, Tallahassee, FL, USA where he is Director of the Institute for Energy Systems, Economics and Sustainability. His research interests include distributed control and reconfigurable systems, real-time system identification, and adaptive control.

Soo-Hwan Cho received his B.S., M.S. and Ph.D. degrees in Electrical Engineering from Korea University, Seoul, Korea, in 2002, 2006 and 2009, respectively. He was an Engineer with Telecommunication Network Division of Samsung Electronics from 2002 to 2004 and a Senior Researcher at Reactor Utilization Division of Korea Atomic Energy Research Institute (KAERI) from 2009 to 2011. Currently, he is a professor of the Department of Energy Grid, Sangmyung University, Seoul, Korea. His research interests include power quality analysis including measurement, detection and classification and signal processing techniques for PQ analysis.

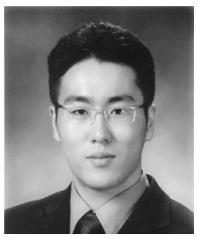

Hyun-Koo Kang received his BS and MS degrees in Electrical Engineering from Seoul National University, Seoul, Korea, in 2005 and 2007, respectively, where he is currently pursuing a PhD degree. His research interests include power quality, distributed energy resources, and operation of microgrids.